Internal–Inertial Waves in a Sargasso Sea Front

RICHARD P. MIED, COLIN Y. SHEN, CLIFFORD L. TRUMP AND GLORIA J. LINDEMANN

Marine Technology Division, Naval Research Laboratory, Washington, DC 20375

(Manuscript received 25 February 1985, in final form 11 March 1986)

ABSTRACT

This work examines the presence of internal–inertial waves in a front in the North Atlantic subtropical convergence zone. Results of Doppler shear profiler and towed thermistor chain surveys are displayed to document the position and magnitude of the front. Objective maps of the total measured velocity are computed and subtracted from the observed velocity fields. The remaining wave signal is processed to yield horizontal (towed) and vertical (dropped) kinetic energy spectra across the front. From these, rotary spectra are also computed along the line of tow and in the vertical to determine the horizontal and vertical anisotropy. It is found that several nearly monochromatic waves are propagating northward and southward from the front with horizontal length scales of ~32–50 km. It was also discovered that the region of anticyclonic frontal vorticity exhibits an excess of downgoing energy at the longest vertical wavelength thus sampled (~50 m), while the region of cyclonic vorticity possesses more upgoing than downgoing energy at the same wavelengths. Vertical and horizontal spectral variances of the total kinetic energy within the region of the front are each enhanced by a factor of about five over the variances outside the front. These results are discussed in the light of recent work by Kunze.

1. Introduction

The North Atlantic subtropical convergence zone is a region in the latitude range 22°–32°N (Voorhis and Hersey, 1964) where the cold water from the North meets the warmer southern water mass. For many years, it was thought that the frontal system resulted from the Ekman convergence of flows induced by the trade winds and the prevailing westerlies to the north. Recently however, Cushman-Roisin (1984) has pointed out that this seems unlikely, and has shown instead that the beta convergence of the thermal flow is a more likely mechanism.

It was also originally believed that the front disappeared during the months of July, August and September, but evidence by Backus et al. (1969) and Colton et al. (1975) indicates that it may be present all year even though it is not discernable from the sea surface temperature. This is an extremely complicated area, however, and at least two fronts have been observed separated by several hundred km (Voorhis, 1969). The occasional existence of more than one front may partly explain the large latitude range in which these fronts have been observed.

The structure of the subtropical convergence zone is complex largely because of the interaction with disturbances which grow in the vicinity of the front. Leetmaa and Voorhis (1978) have observed that alternating cold and warm features can develop on the front so that it assumes a corrugated appearance with wavelengths of order 200 km. More recently, Voorhis and Bruce (1982) have shown that out of these "tongues" of fluid arise submesoscale eddies with diameters of about 50 km. This process appears analogous to that observed by Griffiths and Linden (1981) for laboratory vortices which form from occluded finite amplitude frontal disturbances.

The picture that emerges from the above considerations is that the subtropical convergence zone is a complicated area where a number of mesoscale phenomena are observed. In addition to these larger scale processes, we expect that the energy level of the internal waves will be greatly altered. Mooers (1975a,b) and Olbers (1981) have shown that internal–inertial waves may be trapped in the vicinity of the current jet in a front. Kunze and Sanford (1984) have used expendable current profilers to show rather convincingly that the levels of dropped current spectra are indeed higher in a frontal area in the Pacific, while Kunze (1986) has obtained similar results for spectra in a warm core ring. Using WKB arguments, Kunze (1985) has calculated ray paths in a frontal current jet and demonstrated that some wave rays can undergo many reflections within a frontal region, so that a clear idea emerges of how refraction, reflection and critical layers operate to enhance spectral values of the wave energy there.

In this paper, we present a detailed survey of a front in the North Atlantic subtropical convergence zone, and concentrate upon the internal-inertial waves present. These data, taken with a towed thermistor chain and a Doppler shear profiler, characterize the front and are objectively mapped. The experiment was conducted within a very large meander, and we have observed that both the vertical (dropped) and horizontal (towed) kinetic energy spectra are significantly enhanced in the front. By computing rotary spectra in the vertical and

along the direction of tow, we find the sense of the group velocity in the horizontal and vertical, and these results are discussed in the light of the wave propagation work of Kunze (1985).

2. Experimental data

A frontal survey was conducted during July 19–20, 1981 in the Sargasso Sea west-southwest of Bermuda around (72°W, 31°N). The instruments employed in this survey were an acoustic Doppler shear profiler (DSP) to obtain currents, a towed thermistor chain to measure the temperature field, and a CTD to obtain temperature and salinity as functions of depth. Trump et al. (1985) have employed the DSP and thermistor chain data to characterize the gross frontal structure, but we shall use the DSP observations to describe the internal wave field.

a. Velocity measurements

The DSP system (Hill and Trump, 1982) is mounted on the bottom of the ship with four beams, of 3° width, each pointing down. They are oriented in the fore, aft, port and starboard directions. A 300 KHz acoustic signal is transmitted every 0.62 s with a pulse width of 9.6 ms, and the backscattered return signal is analyzed every 4.8 ms for its Doppler shift. The returns from the four beams are combined with the ship's pitch, roll and heading to produce a vertical profile containing 27 velocity estimates. Each velocity estimate represents the vertical average over 3.34 m depth increments which are centered on depths ranging from 23.3 to 110 m. These velocity profiles are relative to the ship and are quite noisy. When the profiles are averaged for 10 min and combined with ship motion estimates based on Loran-C navigation, profiles of absolute velocities accurate to about 1 cm s^{-1} are obtained.

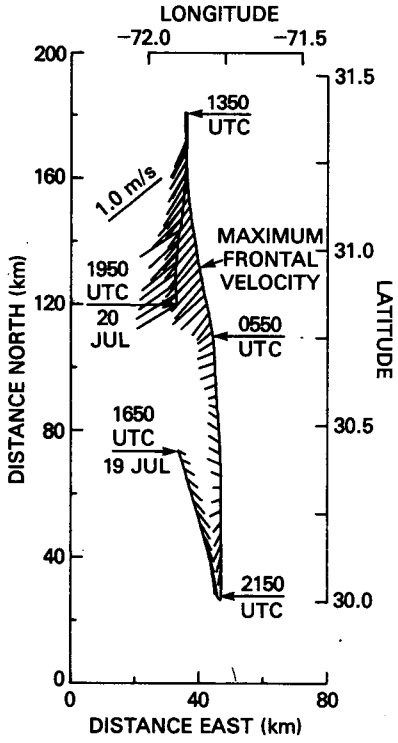

FIG. 1a. Velocity vector diagram of absolute velocity at 40 m depth along the entire survey track for the time interval 19–20 July 1981. The times shown are UTC and occur where the arrow underlying them intersects the ship track. A 1 m s^{-1} velocity is shown for reference. The position of the maximum frontal velocity jet is indicated.

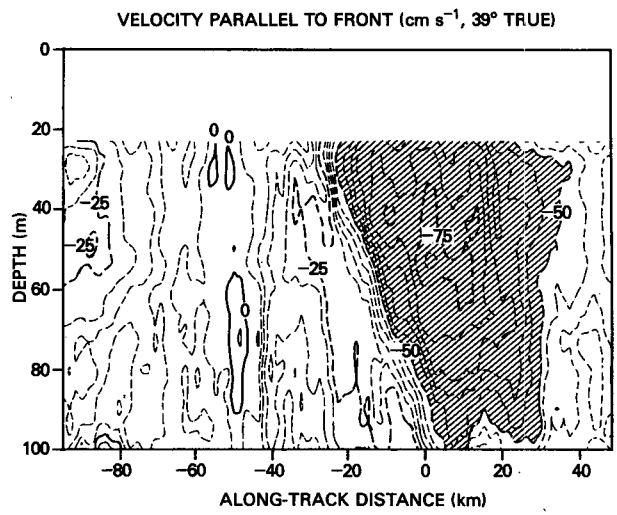

FIG. 1b. A contour plot of the velocity component approximately parallel to the front (along a line 39° clockwise from north, or 39°T). Along-track distance is shown with the origin (position of maximum jet velocity) at 0 km; negative distances are south of this. The negative velocities are directed into the page, and appear as dashed lines. Velocities < −50 cm s^{-1} are shaded to delineate the most energetic portion of the frontal jet. Solid lines represent positive velocities, and the contour interval is 5 cm s^{-1}.

The absolute velocity vectors at 40 m depth along the ship track in the vicinity of the front are shown in Fig. 1a. Three features are significant in this velocity vector picture. The first is that the flow is predominantly toward the southwest, which is in contrast to the generally eastward direction of the subtropical countercurrent. This suggests that the front was crossed where there was a large amplitude meander. Another feature is that that flow is quite strong, having a maximum of order 80 cm s^{-1} in the northern part of the record. And finally, we note the clockwise turning of the velocity vector for the region of the flow in the southern portion where the ship turns, which may suggest the presence of a large-scale inertial feature. This is discussed more fully later (section 5 on horizontal spectra), where an attempt is made to separate the mixed effects of space and time along the ship track.

An advantage in using the DSP to measure velocity is that two-dimensional velocity sections are readily obtained. In Fig. 1b, we show a contour plot of the approximate along-front velocity along a line 39°

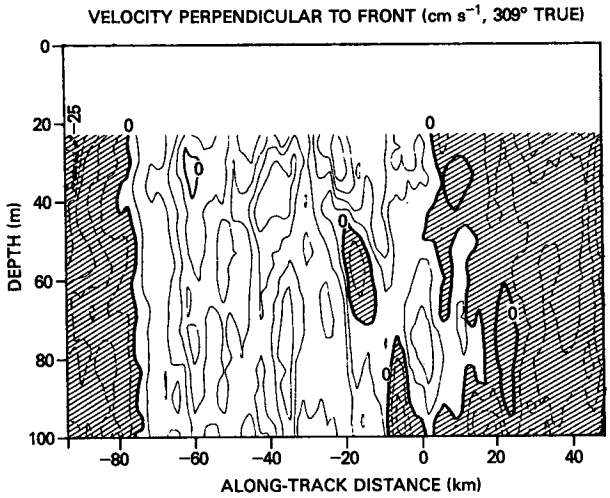

FIG. 1c. A contour map of the velocity component approximately perpendicular to the front (along a line 51° counterclockwise from north, or 309°T). Positive velocities are directed into the page and appear as solid lines. Regions of negative velocity are shaded and the contour interval is 5 cm s^{-1}.

clockwise from north (Trump et al., 1985), measured on the long south-to-north ship's track. The frontal jet is immediately evident as the region where the velocity exceeds 75 cm s^{-1} (and reaches a maximum of 81 cm s^{-1}). The point along the ship's track at which this occurs is marked as the origin (0 km) from which all distances are measured. This serves as a convenient reference point in this and in all of the following figures. In Fig. 1c, we show the contours of fluid velocity in the approximate cross-front direction (along a line 51° counterclockwise from north or 309°T). Without a large coherent signal as in the along-front view, some of the variability associated with the internal–inertial waves is more apparent in the plot of cross-front velocity, as cells of local maximum and minimum velocity.

b. Temperature measurements

The towed thermistor chain (Morris et al., 1983) consists of 180 fast-response thermistors spaced at one-half meter increments along the chain. Although data are taken at 20 Hz, only 4 Hz is used for actual processing. With a typical towing speed of 2.5 m s^{-1}, it is believed that fluctuations with a 60 cm horizontal length can be resolved, while the temperature resolution is considered to be 0.01°C.

The ship traversed the frontal region in the pattern shown in Fig. 1a, that is, from the south to the north. The temperature data (Fig. 2) indicate that the colder water is located to the south of the warm water, which corroborates the previous assertion that the measurements were taken in a large meander. We may objectively analyze the temperature and velocity measurements along the ship track (Fig. 1a) to infer the horizontal structure of these fields.

3. Objective analysis of velocity and temperature fields

The total measured frontal velocity and temperature fields were horizontally mapped using the objective analysis technique described by Bretherton et al. (1976). An isotropic correlation function of the normalized form $C(r) = (1 + \epsilon^2)(1 - \gamma^2 r^2)\exp(-\delta^2 r^2/2)$, which has been found useful in the previous application of the technique (McWilliams, 1976; Freeland and Gould, 1976; and Shen et al., 1986), was used in the present mapping. The noise-to-signal variance ratio ϵ^2 is chosen as 0.3, based upon results of previous mapping experiments in the general area (i.e., MODE and POLYMODE LDE). For simplicity, the zero-crossing parameter (γ^2) is set to zero, but this has a minor influence upon our mapping. The correlation scale $\delta^{-1} = 100$ km is used in the streamfunction and temperature maps in Fig. 3a, b.

At this point, some comments on the limitations of objective analysis are in order. We view this mapping technique as a mechanism to accurately smooth irregularities with length scales much smaller than the autocorrelation length. It shares a marked weakness with any other mapping algorithm, however, because a basic assumption is that the measurements are synoptic. If processes occur on time scales comparable with the survey time, some distortion is very likely to occur. As mentioned before, Fig. 1a indicates a systematic clockwise rotation of the velocity vector in the southern third of the figure, which may be suggestive of near-inertial wave motion. If the wavelengths of the waves do not exceed several tens of kilometers (which is the anticipated result), then the objective analysis should be able to effectively separate the waves and the frontal flow. We thus feel confident in subtracting the velocity data (smoothed by objective mapping) in this figure from the actual measurements to obtain an indication of the

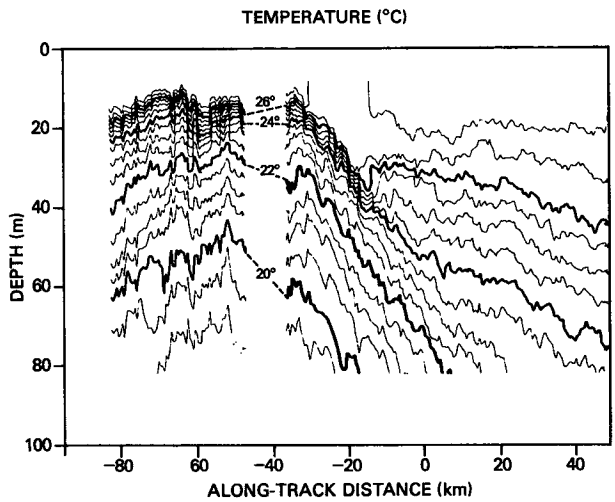

FIG. 2. Temperature along the longest leg (south to north) across the front. Contour interval = 0.5°C, and the gap denotes missing data.

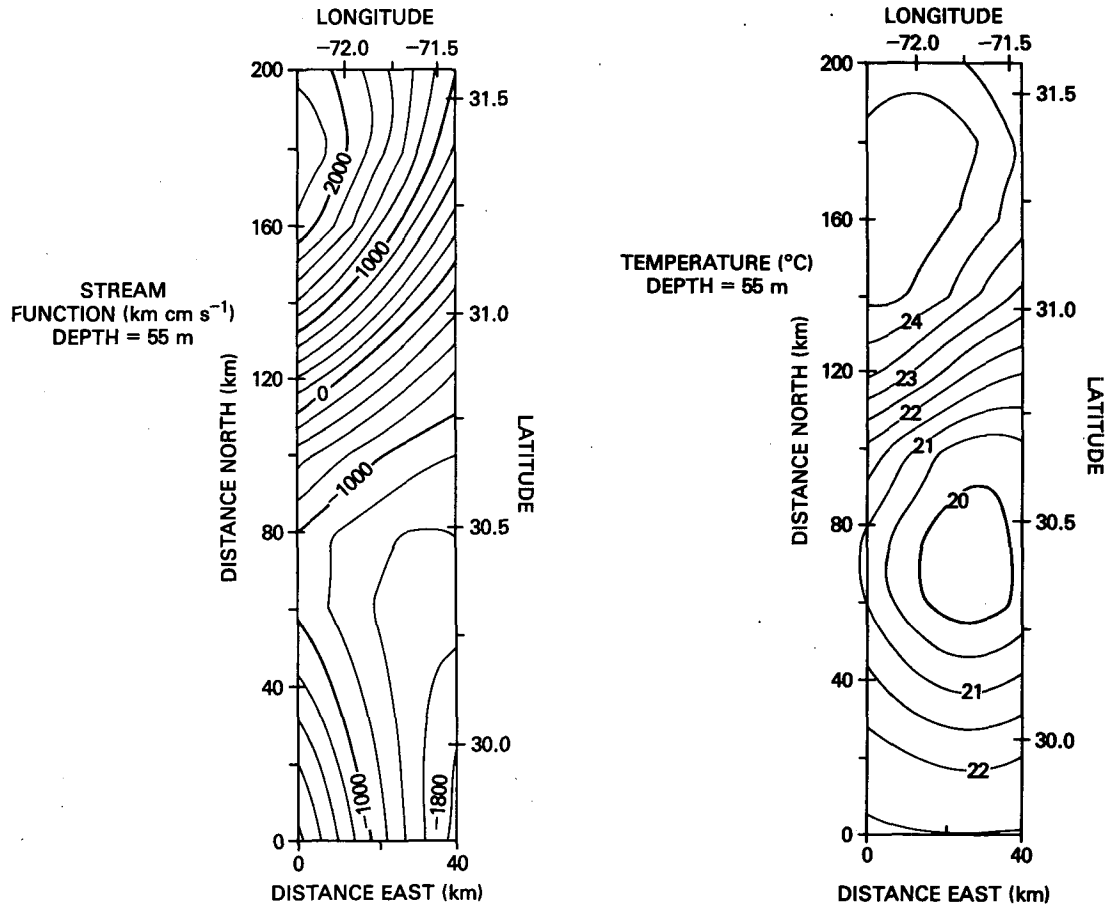

FIG. 3. Objective map of (a) the streamfunction and (b) temperature at 55 m depth.

wave field present. First, however, it will be useful to review some information regarding internal waves in fronts.

4. Internal waves in fronts

In the previous sections we have dealt primarily with the properties of the large-scale flow, alluding only briefly to the presence of the internal waves. The influence of the mesoscale upon the waves can be significant, however, as has been shown by Mooers (1975a,b), Olbers (1981) and Kunze (1985). The study of Kunze has demonstrated the importance of the density stratification and of the horizontal and vertical shear. In particular, he shows that downgoing waves may be trapped in regions of surface-intensified negative vorticity [$\zeta = (\partial V/\partial x) - (\partial U/\partial y)$], where the horizontal velocity is (U, V) and positive (x, y) are the easterly and northerly directions, respectively. As the waves propagate downward in this environment the vorticity becomes smaller and the effective Coriolis frequency ($f + \zeta/2$) increases. Being constrained by their dispersion relation, the waves adjust by decreasing their vertical wavelength. A critical layer ensues in which the vertical group velocity vanishes and the wave is amplified. A similar scenario takes place for upgoing waves propagating into regions of surface-intensified positive vorticity.

In order for a wave to be amplified, then, the sign of the vorticity of the mesoscale field must be closely linked with the vertical directionality of the internal wave field. Careful examination of the special cross-front propagation case (Mooers, 1975a) indicates that local wave trapping relies upon a wave-guide effect involving the frequency of the waves, the horizontal and vertical density gradients, and the vertical vorticity. However, order-of-magnitude estimates using data in the present study indicate that the most important quantity is the vorticity. The calculation of this vorticity field is a straightforward task requiring evaluation of the Laplacian of the streamfunction field (ψ) from an objective map. In Fig. 4, we show contours of $\nabla^2\psi$ at a depth of 55 m with the ship track superimposed. The point where the vorticity changes sign is not the zero km location in the figures. This latter point only designates the position of maximum along-front flow, while ignoring any cross-front contribution.

From Fig. 4, we see that the southern portion along

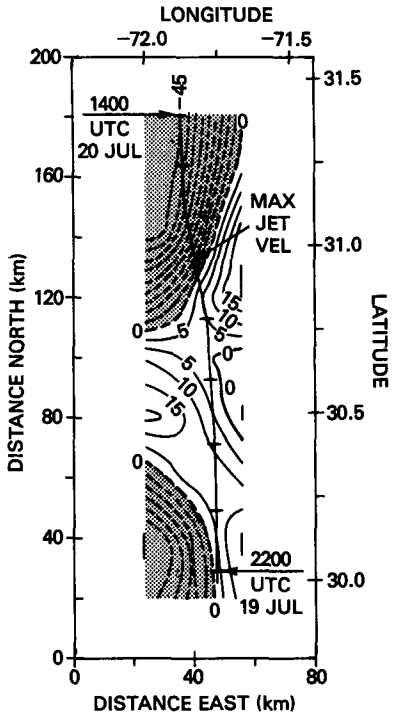

FIG. 4. Contours of vorticity $\nabla^2\psi$ at 55 m depth for the frontal flow. Negative regions are shaded and the contour interval = 5×10^{-6} s^{-1}. The ship track is also shown with tic marks at two hour increments.

the cruise track has positive vorticity, while the vorticity is negative in the north. Based upon the preceding discussion, we expect that the northern part of the frontal region will be a favorable site for downgoing energy, while upgoing energy will tend to be favored to the south of the front. These tendencies are, in fact, observed, and will be presented in section 6. In the next section, however, we shall present the rotary spectra of horizontal kinetic energy and use them to determine how much energy is propagating northward or southward.

5. Horizontal spectra of horizontal kinetic energy

In this section, we shall examine the variation of the horizontal (or towed) spectrum of the horizontal kinetic energy. To our knowledge, horizontal spectra of internal wave kinetic energy have not been reported previously. The calculation of these spectral representations is possible because the DSP provides a continuous horizontal record of the velocity at many depth bins. In addition, we have calculated clockwise and anticlockwise horizontal spectra to discern how much of this energy is flowing horizontally into or away from the front.

To obtain an impression of the physical processes observed in the front, we must examine the velocity data from the DSP. We resolve this into the approximate along-front and cross-front velocities (39° and 309°T, respectively) in Fig. 5a, and we present the two velocity components; these are absolute velocities at 50 m depth which contain both the frontal flow and the internal waves. Notice that the along-front velocity is dominated by a fairly broad jet with a velocity half-width that extends over about 80 km of cruise track. Some fluctuation due to waves is present in this, but the dominant signal is the frontal current. On the other hand, the cross-front velocity record shows little evidence of the frontal velocity (as expected), but it is dominated instead by wave motion with length scales of tens of km.

The results of the objective analysis for the velocities are also shown in Fig. 5b. Here, we display the cross-front and along-front velocities (averaged from the 45 and 55 m maps), which we then subtract from the raw data to obtain the signature of the wave-related velocities parallel to—and perpendicular to—the front (Fig. 5c). The regions of positive and negative vorticity are shown in Fig. 5b. The wave information in Fig. 5c may be displayed in a more conventional manner by presenting a vector diagram of the wave-related current along the ship track (Fig. 6a). We can see that the current vector varies in magnitude and phase as the ship moves through the front; however, these are in situ velocities, each measured at different times as the ship encounters them. A property of inertial waves in the Northern Hemisphere is that their velocity vector always rotates clockwise with time at a given depth. In order to infer the velocity field of the waves at an instant, we rotate the hodograph vector in an anticlockwise direction by an amount $f \cdot \Delta t$, where $f = 7.49 \times 10^{-5}$ s^{-1} (the local Coriolis frequency) and Δt is the time required for the ship to travel from the extreme left of the figure (−96 km) to a position along the track. Viewed in this fashion, the inertially rotated velocity field gives a fairly accurate picture of the near-inertial field as it would have appeared had we been able to take a snapshot of it at one instant. This snapshot should then be amenable to physical interpretation.

In order to understand the significance of features in Fig. 6b, we note that the local $+x$ and $+y$ velocities and the group velocity for an inertial wave are given by LeBlond and Mysak (1978) as

$$(u, v) = \frac{-W(N^2-\omega^2)}{\omega k_z(\omega^2-f^2)}(k_x\omega + ifk_y, k_y\omega - ifk_x) \times \exp[i(k_x x + k_y y + k_z z - \omega t)]$$

$$\mathbf{c}_g = \frac{k_z^2(N^2-f^2)}{|k|^3(f^2k_z + N^2k_H^2)^{1/2}}(k_x, k_y, -k_H^2/k_z)$$

where N is the Brunt–Väisälä frequency, $k = (k_H, k_z)$, $k_H = (k_x, k_y)$, $\omega^2 = (N^2k_H^2 + f^2k_z^2)/k^2$ has been used and the vertical velocity is assumed to be of the form $w = W \exp i(\mathbf{k} \cdot \mathbf{x} - \omega t)$. We may calculate

$$\frac{\mathrm{Re}u}{\mathrm{Re}v} = \cot^{-1}(\mathbf{k} \cdot \mathbf{x} - \omega t + \phi)$$

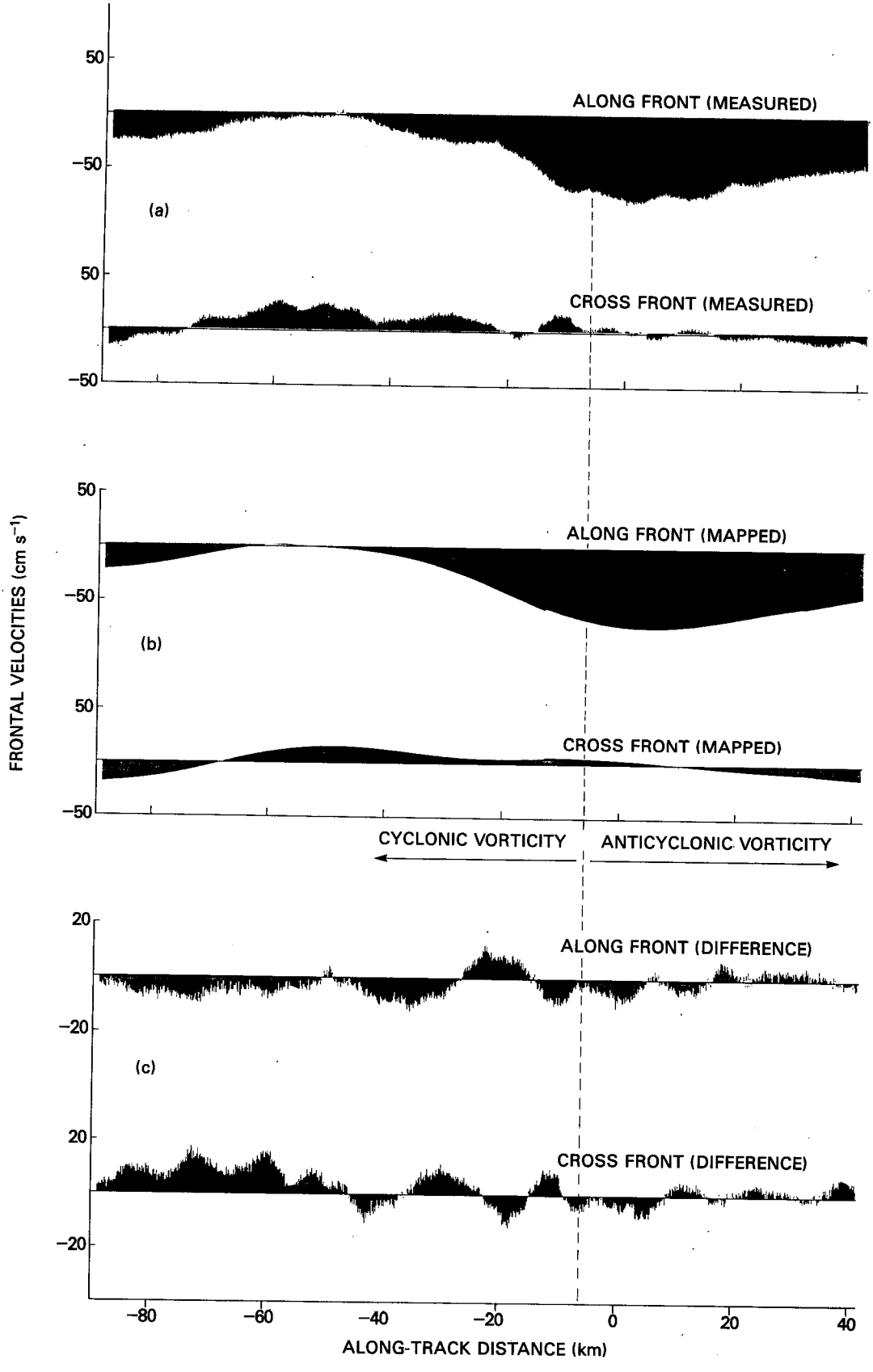
50
ALONG FRONT (MEASURED)
−50
(a)
50
CROSS FRONT (MEASURED)
−50
50
ALONG FRONT (MAPPED)
−50
(b)
50
CROSS FRONT (MAPPED)
−50
FRONTAL VELOCITIES (cm s⁻¹)
CYCLONIC VORTICITY
ANTICYCLONIC VORTICITY
20
ALONG FRONT (DIFFERENCE)
−20
(c)
20
CROSS FRONT (DIFFERENCE)
−20
−80
−60
−40
−20
0
20
40
ALONG-TRACK DISTANCE (km)

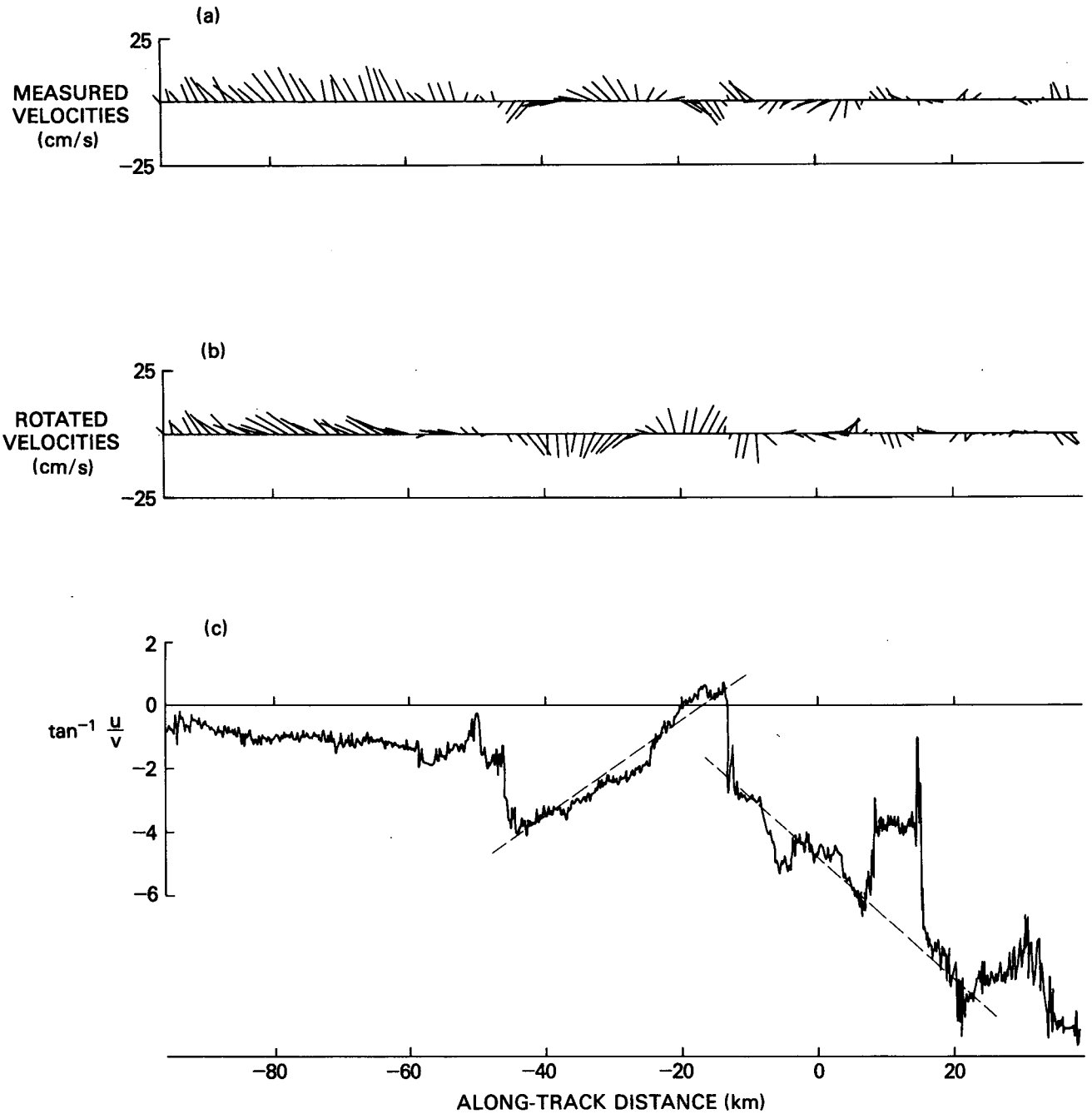

FIG. 6a. Measured velocities at 50 m depth along the ship track, proceeding from south to north.
FIG. 6b. Rotated velocities at 50 m depth.
FIG. 6c. $\tan^{-1}u/v$ at 50 m depth, where u and v are the rotated velocities in Fig. 6b. $\tan^{-1}u/v$ increasing from left to right indicates clockwise turning of the velocity vector in Fig. 6b.

FIG. 5a. Observed velocity components in the along-front (39°T) and cross-front (309°T) directions at 50 m depth.
FIG. 5b. Objective analysis representation of velocity components in the along-front and cross-front directions at 50 m depth. The regions of cyclonic and anticyclonic vorticity are shown.
FIG. 5c. Difference of the observed and mapped velocities (assumed to be attributed to waves) at 50 m depth.

where $\phi = \cos^{-1} k_x/|k_H|$ and we have put $\omega \sim f$. For a constant depth and time (z and t fixed), increasing horizontal phase ($k_x x + k_y y$) means that Reu/Rev must decrease (i.e. rotate in an anticlockwise sense). Because k_H and the *horizontal* group velocity are colinear, we may identify the direction of the horizontal group velocity as the direction in which the hodograph vector rotates *anticlockwise* in a horizontal direction.

In Fig. 6b, we see that as we go from −14 to −46 km, the vectors rotate anticlockwise. As shown above, this indicates the presence of a southward (toward more negative distances) propagating wave. The trend in this portion of the record is unambiguous, but it is difficult to discern other patterns in the more noisy portion of Fig. 6b. To do this, we plot $\tan^{-1}u/v$ for the ship track in Fig. 6c. When $\tan^{-1}u/v$ increases along the ship track, the rotated velocity vectors in Fig. 6b are turning clockwise as we go from left to right along the curve.

Three segments of the curve in Fig. 6c are interesting because they show pronounced tendencies. The first is the trend from −96 to −46 km, which corresponds to the feature noted in the lowest third of Fig. 1a. The anticlockwise phase trend (going from left-to-right) changes by only about 1 radian, indicating a very long wavelength along the ship track. It may be that this wave is propagating across the cruise path (i.e., east–west). The remaining two trends are designated with dashed lines to indicate their slopes. Their extents are −46 to −14 km (a southward propagating wave) and −14 to +20 km (northward propagating). This second wave appears to have a number of places where the phase is disrupted, but the overall trend seems present nevertheless.

The direction of propagation and the location of these two waves with respect to the front indicates that they are being radiated away from the front. Because the front was undergoing a large-amplitude meander (Fig. 3a) when we crossed it, these inertial waves may have been radiated in an adjustment process.

The fitting of an objectively analyzed velocity field has been performed for the five equally spaced depths in the 35–75 m depth range. These objective maps are used to detrend the velocity data in the same fashion as those at the 50 m depth in Fig. 5 (the average of the 45 and 55 m maps), so that we have five time series of wave-related velocity records as the front is traversed. Horizontal clockwise (CW), anticlockwise (ACW) and total kinetic energy spectra are taken after cosine-tapering 39.8 km segments of the inertially rotated data. These horizontal rotary spectra allow us to quantify the observations of the energy in the southward and northward propagating waves. We have used a number as large as 39.8 km because the noise floor in the spectra renders them useless for wave numbers > (2.5 km)$^{-1}$. The interval 2.5–39.8 km thus gives at least a decade over which a meaningful variance can be computed. The average of the spectra from the five depths then gives an approximation to the spectrum for that 39.8 km segment. The previous discussion suggests that the relative proportion of energy contained in CW and ACW motions should vary along the ship track. In Fig. 7, we have plotted CW, ACW and total kinetic energy spectra for three equally-spaced locations across the front: two within the cyclonic region and one within the region of anticyclonic frontal vorticity.

We see that south of the front (a 39.8 km window centered at −46.2 km), there is more clockwise than anticlockwise energy at the longer wavelengths. This indicates that more energy is propagating southward than northward there, although this is not immediately apparent from Fig. 6b, c. Within the front (−23.7 km, or where the isotherms have the largest slope) the energy

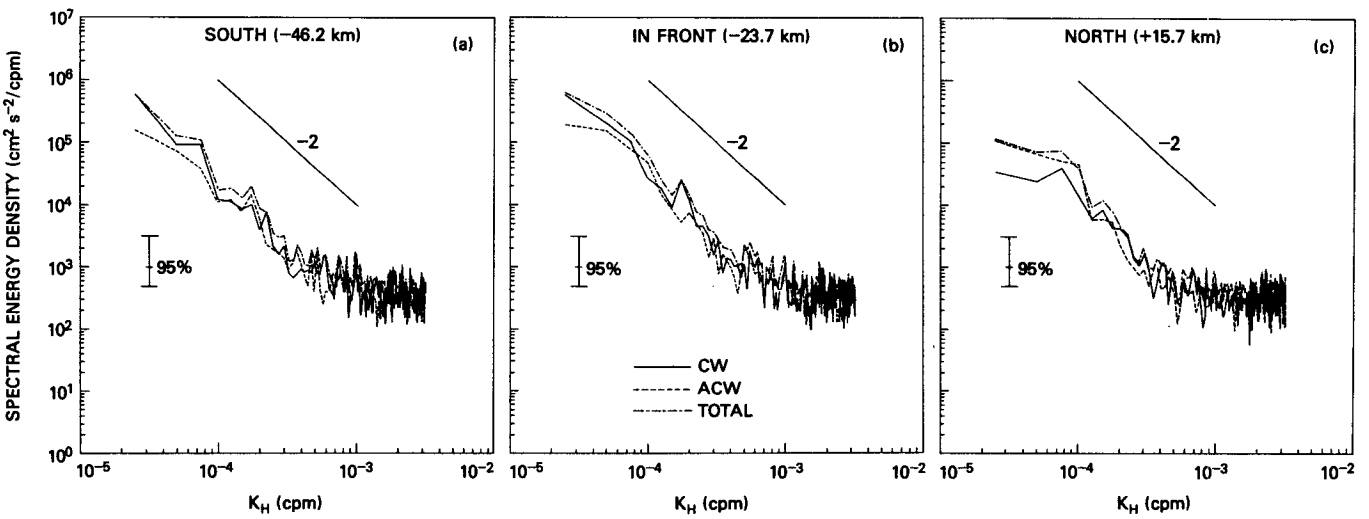

FIG. 7. Horizontal kinetic energy spectra at three positions across the front: south (−46.2 km), within (−23.7 km) and north (+15.7 km). Each position is the center of a 39.8 km interval.

in the longest wavelengths is more evenly distributed between the CW and ACW spectra. North of the front (+15.7 km) the ACW spectrum dominates.

We note, however, that all of the spectra are contained within a 95% confidence window, so that we cannot say with great certainty that one spectrum differs significantly from another. Nevertheless, when spectral variances are introduced below, we can see that they vary systematically along the ship track and that they seem to show spectral levels are enhanced within the front.

For comparison, a spectral slope of -2 is drawn also. This slope seems to be a reasonable representation of the spectral roll-off which continues until the spectrum reaches the noise level and is in qualitative agreement with the GM 79 model (Munk, 1981; Desaubies, 1976). This noise level is seen to be of the order 3×10^2 cm^2 s^{-2}/cpm, which is consistent with an instrument uncertainty of ~ 1.0 cm s^{-1} in a ten minute averaged record over this bandwidth (1.0^2 cm^2 s^{-2}/3.0×10^{-3} cpm $\sim 3 \times 10^2$ cm^2 s^{-2}/cpm). These spectra appear to intersect this level at a wavenumber of $\sim 4 \times 10^{-4}$ cpm, or 2.5 km.

A convenient measure of the way in which the CW, ACW and total energy spectra behave as we traverse the front may be obtained by forming their energy in the horizontal wavelength band 2.5–39.8 km (Fig. 8). This 39.8 km band is moved in 5 km increments across the front to generate the curves in this figure. We note that the ACW energy (northward propagating waves) has two local peaks (-60 and -10 km) which are present because of the features with anticlockwise rotation (see Fig. 6c). The CW energy has a local maximum around -25 km. Figure 6c indicates the presence of an extensive inertial feature with pronounced southward propagation.

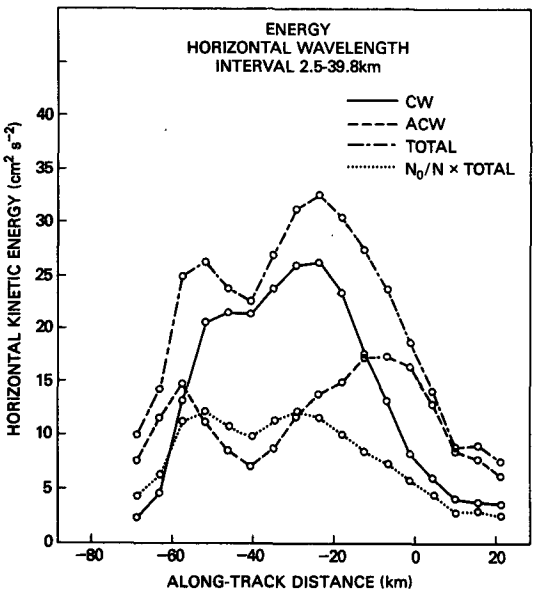

FIG. 8. CW, ACW, total and scaled horizontal kinetic energy in the 2.5–39.8 km wavelength range along the ship track. The energy is computed by moving this sampling window in 5 km increments along the long south-to-north survey track.

These enhanced CW and ACW spectra sum to yield a total horizontal kinetic energy which has near-front values four or five times greater than those away from the front. By multiplying this energy by N_0/N ($N_0 = 3$ cph), we may account for the variation of the Brunt–Väisälä frequency and its influence upon the spatial variation of the wave energy. While the magnitude of the energy peaks is diminished somewhat, the curve still indicates an enhancement of the towed horizontal kinetic energy in the area of the front.

6. Vertical spectra of horizontal kinetic energy

In this section, we examine the vertical CW, ACW and total kinetic energy spectra of the horizontal velocity, and their variation across the front. Although the expected vertical wavelengths of the dominant inertial frequency waves are several hundred meters (Sanford, 1975; Leaman and Sanford, 1975), some information is contained in the larger wavenumbers, and we may sample information in these small length scales. The DSP can measure velocities to depths of 110 m; however, the instrument relies upon the scattering from suspended material. A reduction in the density of scatterers was noted in the deepest portions of the northern section of the tow and this yielded unreliable information for the lowest 30 m of the acoustic return. As a consequence of this, we have confined our interest to velocity fluctuations over a 50 m depth range (29.4–79.4 m). While this may seem to be overly restrictive in view of the energy expected to be present in larger scales, some interesting trends have been observed. Moreover, calculation of the vertical spectrum is used to more accurately delineate the enhanced wave energy area. The 39.8 km horizontal window used in the towed spectra tended to average over a region much larger than that in which the waves may have exhibited local energy peaks.

To obtain the vertical (dropped) rotary spectra of horizontal wave energy, the data has been treated in a fashion quite similar to that of the previous section. First, however, we obtain a mean in the following fashion. The objective analysis maps at the five depths 35, 45, 55, 65 and 75 m below the surface each give a value of the along-front and cross-front velocities. These five values for each of the velocity profiles are least-squares fitted to a polynomial in depth z of the form, $a_0 + a_1 z + a_2 z^2$; this defines mean velocity profiles which are subtracted from the DSP velocities (Fig. 9). After removing the mean and cosine-tapering, rotary spectra are taken. Five of these dropped spectra, separated by one minute (~ 150 m), are averaged to form the spatial realizations shown in Fig. 10.

The rotary spectra in Fig. 10 indicate that the CW

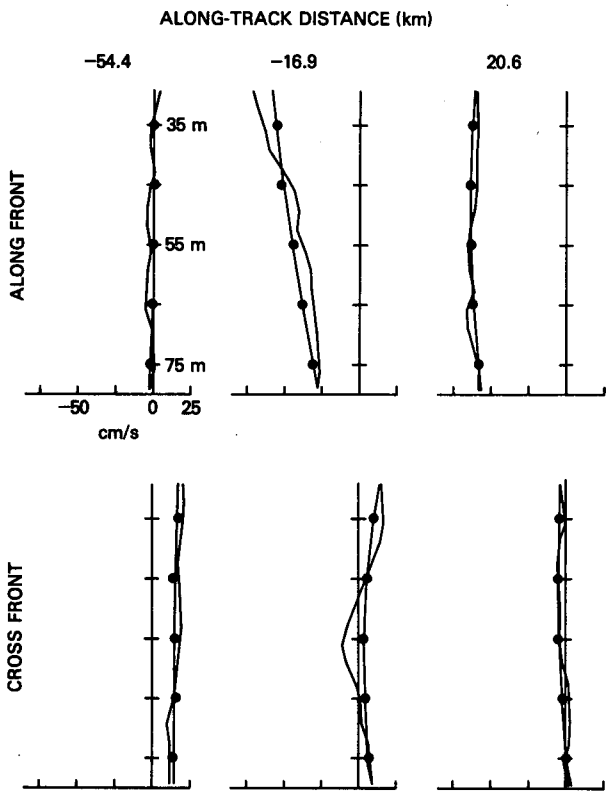

FIG. 9. Absolute velocities in the along-front and cross-front directions at different along-track distances (km). The objectively mapped velocities have been marked with a dot and these values have been fitted with a second-order polynomial, also shown. The difference of the observed absolute velocities and the objective ones is taken to be the wave signal.

spectra north (20.6 km) and south (−54.4 km) of the front are about the same level and roll off as K_v^{-2}. The ACW spectra behave similarly at the same locations. In the vicinity of the front (−16.9 km), however, both the CW and the ACW spectra are significantly higher in the smaller wavenumbers, and the roll off appears steeper than −2. These are only realizations at three locations, and a better impression of the behavior of the energy over the front is obtained by summing the energy in the vertical wavelength band 6.3–50 m. These energies are shown in Fig. 11, and some interesting trends are seen. The first is that both the CW and ACW energies show a sharp peak at about −20 km, and these peaks have widths at their half heights of 10–20 km. These peaks could be caused by the trapping of waves which propagate against the current (Olbers, 1981; Kunze, 1985). As we cannot discern the directions of the wavenumber in the cross-track direction, we cannot rule out this possibility. On the other hand, the occurrence of each peak in more or less the same location within the front may support the hypothesis of generation by a geostrophic adjustment process, which was postulated to explain the horizontal radiation observed in Fig. 6c.

The second fact in Fig. 11 is that there are several places where the one energy exceeds the other. To identify these locations, we selected two (arbitrary) criteria to decide whether the inequality was significant. We designated with a vertical arrow these locations where the energies satisfied both of the following:

1) the one exceeded the other by a factor of *at least* two; and,
2) that point was accompanied by several others; that is, it was not a single occurrence.

Arrows pointed upward indicate a surplus of upgoing energy, while arrows directed downward designate more downgoing than upgoing. We see that the observations of downgoing energy occurred in an anticyclonic frontal vorticity area, while episodes of upgoing energy were confined to regions of cyclonic frontal vorticity.

Unlike the broad peak of the towed spectral variance (Fig. 8), the dropped rotary kinetic energy spectra show fairly narrow enhanced regions of 10–20 km. The reason for this is fairly clear: The vertical measurements represent a more local view of the wave energy, while the towed measurements are averaged horizontally over 39.8 km and so generate a much broader energy peak.

Moreover, the region south of the front has more energetic waves than that north of the front (Fig. 6). The peak in the total towed horizontal energy (Fig. 8) is thus biased more southward than the corresponding dropped energy peak (Fig. 11). This is because the towed computation averages in these more energetic waves, drawing the peak southward.

7. Discussion and conclusions

The Doppler shear profiler data in section 2 reveals that the internal wave currents in the vicinity of the front have the appearance of cells of velocity with vertical extents of tens of meters and horizontal extents of tens of kilometers.

In order to examine these waves, we have analyzed the data in both the horizontal and in the vertical. The appearance of the vector and phase plots in Fig. 6b, c suggests the presence of several large waves with length scales of 32–50 km in the north–south direction. The inertial wave portion of the spectrum in this area of the front is dominated by identifiable, large-scale waves, rather than an ensemble of smaller scale ones. The length scales of these waves are smaller than, or about the same size as, the width of the frontal jet (~50 km). This result appears to be in qualitative agreement with an observation by Kunze and Sanford (1984) who reported near-inertial waves with length ~20 km in a frontal region ~ 20 km wide. Because of the presence of these large waves in the horizontal velocity record, we noted a spectral roll-off steeper than −2 at the lowest wavenumbers.

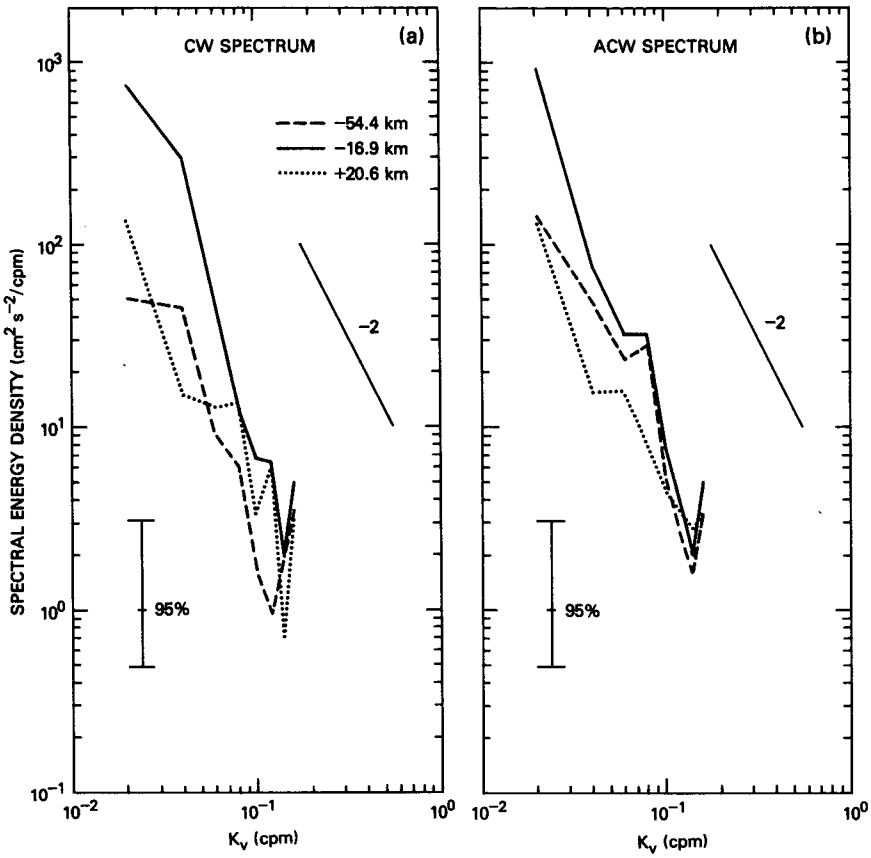

FIG. 10. Vertical rotary spectra at locations along the ship track: −54.4, −16.9 and +20.6 km.

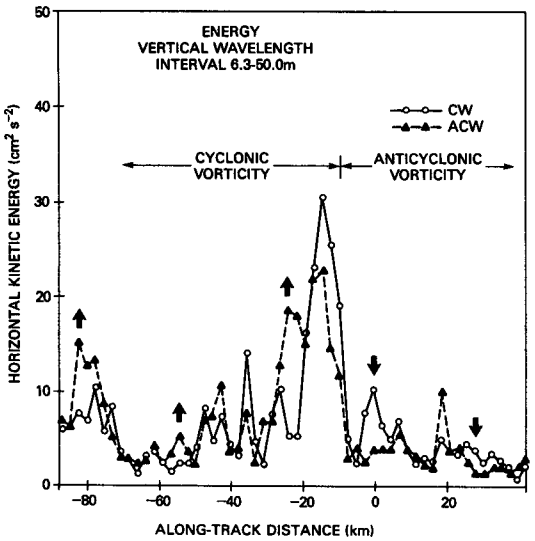

FIG. 11. Energy in vertical profiles of CW and ACW horizontal kinetic energy (in the 6.3–50.0 m wavelengths bin) along the long south–north ship track. Bold arrows indicate a dominance of either upgoing (↑) or downgoing (↓) energy. See text for explanation of the two criteria used. The regions of cyclonic and anticyclonic frontal vorticity are indicated.

We have also calculated vertical rotary spectra to determine how much energy is propagating upward, and how much propagates downward. Even though our maximum aperture is 50 m, which is rather short in relation to previously observed vertical wavelengths, we have found some interesting trends. In particular, the cyclonic vorticity region of the front showed three episodes of upgoing energy (a dominance of ACW over CW), while the anticyclonic area tended to exhibit two locations where downgoing energy was favored (more CW than ACW). Although we must necessarily consider the sources of these very small-scale waves uncertain, the propagation directions in the particular background vorticity in which they were observed is consistent with the calculation of critical layer amplification made by Kunze (1985).

We have concentrated almost exclusively on velocity data in this paper. Because we also employed a towed thermistor chain with 0.5 m sensor spacing, information can be obtained about the temperature signatures of motions on this scale. In a companion paper (Shen and Mied, 1986), observations have been made of the occurrence frequency of the overturning of the ambient temperature field by a local advective or shear insta-

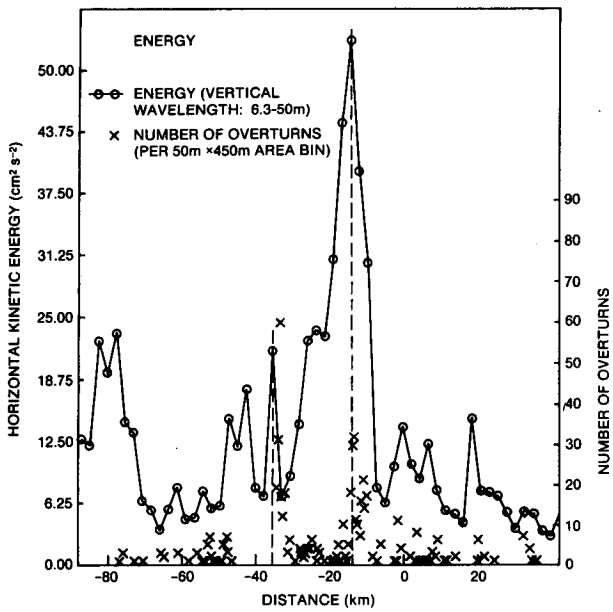

FIG. 12. The total energy (CW + ACW) in the 6.3–50.0 m wavelength bin, and the number of temperature overturns in a box of length 450 m and height 50 m (from Shen and Mied, 1986). The two locations with large overturn count are seen to occur near where these high wave energies are marked with dashed vertical lines.

bility of the internal wave field. Based on the results of that paper, we have counted the number of local temperature overturns in a series of contiguous boxes with heights of 50 m and lengths of 450 m. We relate this spatial overturn distribution to the total horizontal kinetic energy (CW + ACW) in the 6.3–50 m vertical wavelength band (Fig. 12). Regions of large overturn count are seen to correspond *approximately* to regions where the wave energy is high. Clearly, the effectiveness of the wave field in producing shearing or advective instability is dependent upon the spectral content of the wave signal as well as the relative phases of these waves. Nevertheless, the *tendency* of energetic wave fields to produce local density overturns has been observed in the pseudo-spectral numerical calculations of Shen and Holloway (1986), and this tendency is in qualitative agreement with the results reported here.

Acknowledgments. The authors are grateful to J. P. Dugan, T. M. Joyce, G. O. Marmorino, E. Kunze and T. B. Sanford for helpful discussions during the preparation of this work, and to B. McMorrow and C. Pasquini for typing the manuscript.

REFERENCES

Backus, R. H., J. E. Craddock, R. L. Haedrich and D. L. Shores, 1969: Mesopelagic fishes and thermal fronts in the western Sargasso Sea. *Mar. Biol.*, **3**, 87–106.

Bretherton, F. P., R. E. Davis and C. B. Fandry, 1976: A technique for objective analysis and design of oceanographic experiments applied to MODE-73. *Deep-Sea Res.*, **23**, 559–582.

Colton, J. B., D. E. Smith and J. W. Jossi, 1975: Further observations on a thermal front in the Sargasso Sea. *Deep-Sea Res.*, **22**, 433–439.

Cushman-Roisin, B., 1984: On the maintenance of the subtropical front and its associated countercurrent. *J. Phys. Oceanogr.*, **14**, 1179–1190.

Desaubies, Y. J. F., 1976: Analytical representation of internal wave spectra. *J. Phys. Oceanogr.*, **6**, 976–981.

Freeland, H. J., and W. J. Gould, 1976: Objective analysis of mesoscale ocean circulation features. *Deep-Sea Res.*, **23**, 915–923.

Griffiths, R. W., and P. F. Linden, 1981: The stability of vortices in a rotating, stratified fluid. *J. Fluid Mech.*, **105**, 283–316.

Hill, R. H., and C. L. Trump, 1982: An interim Doppler shear profiler: Experimental results. NRL Memo. No. 4920, Naval Research Laboratory, Washington, DC, 112 pp.

Kunze, E., 1985: Near-inertial wave propagation in geostrophic shear. *J. Phys. Oceanogr.*, **15**, 544–565.

——, 1986: The mean and near-inertial velocity fields in a warm core ring. *J. Phys. Oceanogr.*, **16**, 1444–1461.

——, and T. B. Sanford, 1984: Observations of near-inertial waves in a front. *J. Phys. Oceanogr.*, **14**, 566–581.

Leaman, K. D., and T. B. Sanford, 1975: Vertical energy propagation of inertial waves: A vector spectral analysis of velocity profiles. *J. Geophys. Res.*, **80**, 1975–1978.

LeBlond, P. H., and L. A. Mysak, 1978: *Waves in the Ocean.* Elsevier, 602 pp.

Leetmaa, A., and A. D. Voorhis, 1978: Scales of motion in the subtropical convergence zone. *J. Geophys. Res.*, **83**, 4589–4592.

McWilliams, J. C., 1976: Maps from the mid-ocean dynamic experiment, Part 2. Geostrophic streamfunction. *J. Phys. Oceanogr.*, **6**, 810–827.

Mooers, C. N. K., 1975a: Several effects of a baroclinic current on the cross-stream propagation of inertial-internal waves. *Geophys. Fluid Dyn.*, **6**, 245–275.

——, 1975b: Several effects of baroclinic currents on the three-dimensional propagation of inertial–internal waves. *Geophys. Fluid Dyn.*, **6**, 277–284.

Morris, W. D., J. P. Dugan, B. S. Okawa, C. W. Martz and E. E. Rudd, 1983: Towed thermistor system for marine research. *IEEE Proc. Third Working Symp. on Oceanographic Data Systems.* IEEE Computer Society, Woods Hole, 147–153.

Munk, W., 1981: Internal waves and small scale processes. *Evolution of Physical Processes.* B. A. Warren and C. Wunsch, Eds., 264–291.

Olbers, D. J., 1981: The propagation of internal waves in a geostrophic current. *J. Phys. Oceanogr.*, **11**, 1224–1233.

Sanford, T. B., 1975: Observations of the vertical structure of internal waves. *J. Geophys. Res.*, **80**, 3861–3871.

Shen, C. Y., and G. Holloway, 1986: A numerical study of the frequency and energetics of nonlinear internal gravity waves. *J. Geophys. Res.*, **91**, 953–973.

——, and R. P. Mied, 1986: Statistics of internal wave overturning from obervations of upper ocean temperature. *J. Phys. Oceanogr.*, **16**, 1763–1776.

——, J. C. McWilliams, B. A. Taft, C. C. Ebbesmeyer and E. J. Lindstrom, 1986: The mesoscale structure and evolution of dynamical and scalar properties observed in the Northwestern Atlantic Ocean during the POLYMODE local dynamics experiment. *J. Phys. Oceanogr.*, **16**, 454–482.

Trump, C. L., B. S. Okawa and R. H. Hill, 1985: The characterization of a midocean front with a Doppler shear profiler and a thermistor chain. *J. Atmos. Oceanic Technol.*, **2**, 508–516.

Voorhis, A. D., 1969: The horizontal extent and persistence of thermal fronts in the Sargasso Sea. *Deep-Sea Res.*, **16**(Suppl.), 331–337.

——, and J. G. Bruce, 1982: Small-scale surface stirring and frontogenesis in the subtropical convergence of the western North Atlantic. *J. Mar. Res.*, **40**(Suppl.), 801–821.

——, and J. B. Hersey, 1964: Oceanic thermal fronts in the Sargasso Sea. *J. Geophys. Res.*, **69**, 3809–3814.